Tellus (1989), *41A*, 1–17

Polar lows as arctic hurricanes

By KERRY A. EMANUEL, *Center for Meteorology and Physical Oceanography, Massachusetts Institute of Technology, Cambridge, MA 02139, USA* and RICHARD ROTUNNO, *National Center for Atmospheric Research, Boulder, CO 80307-3000, USA*

(Manuscript received 12 October 1987; in final form 10 March 1988)

ABSTRACT

Satellite observations of the polar oceans have revealed the presence of small, intense vortices that often resemble hurricanes, having clear central eyes surrounded by deep convective clouds. Recent aircraft and dropsonde data also show that these storms, like hurricanes, occur within deep moist adiabatic atmospheres and possess warm cores. We propose that at least some polar lows are indeed arctic hurricanes. Using a recently developed theoretical model of the mature hurricane, we show that the observed difference between the moist entropy of the troposphere and that representing saturation at sea surface temperature can sustain moderately intense hurricanes. Unlike the environments of tropical hurricanes, much of this moist entropy difference results from an air–sea temperature difference. Numerical experiments using an axisymmetric nonhydrostatic model confirm that intense hurricanes can develop in environments typical of those in which polar lows are observed to develop. Due to the relatively large values of the Coriolis parameter, these storms have smaller diameters than do hurricanes. The experiments also show that the deep, cold cut-off lows which create favorable thermodynamic environments for polar lows also inhibit their development because of the large intertial stability of their circulations. Finally, we show that, like hurricanes, surface flux-driven polar lows cannot arise spontaneously, but require an independent and presumably non-axisymmetric dynamical mechanism for their initiation.

1. Introduction

Bergeron (1954) was perhaps the first to remark on the special properties of cyclogenesis over relatively warm water in winter. Noting that certain occluded cyclones were rejuvenated while passing over the North Sea and Baltic, he coined the term "extratropical hurricane" to describe these oceanic cyclones. Bergeron's early intuition is well served by recent satellite observations (e.g., see Rasmussen, 1985) that reveal small, intense vortices with clear eyes surrounded by deep cumulonimbi, and by research aircraft observations (Shapiro et al., 1987) which show that like their tropical cousins, polar lows have warm, high θ_e cores.

On the other hand, storms of this kind nearly always form in highly baroclinic environments and, unlike in the case of tropical cyclones, are preceded by powerful upper tropospheric precursors (Businger, 1985). Many polar lows appear to develop near, if not at, the location of the center of deep, cut-off cyclones (Rasmussen, 1985; Businger, 1985), while other small-scale vortices appear to form in polar air within strong zonal flow aloft (Reed, 1979). While it is agreed that all such cyclones form within convectively active polar air, the variety of baroclinic environments in which the storms originate has led to a proliferation of both terminology to describe them and theories for their case. Some, such as Reed (1979) and Harrold and Browning (1969) have argued that baroclinic instability is the principle mechanism, with the reduced static stability of the low-level atmosphere responsible for both the small scales and rapid time evolution of the cyclones (Staley and Gall, 1977). Others, such as Rasmussen (1979, 1985), proposed that polar lows are the result of conditional instability of the second kind (CISK), perhaps acting in conjunction with baroclinic processes.

The importance of both baroclinic processes and surface fluxes has been highlighted in recent numerical simulations of polar lows. Sardie and Warner (1985) used the NCAR/PSU mesoscale model to simulate observed polar lows over both the Atlantic and Pacific Oceans. They concluded that (moist) baroclinic processes were operative in each case and dominated the development of the Pacific cyclone, while surface heat fluxes were essential in producing a disturbance of the observed amplitude in the Atlantic case. Grønås et al. (1987) used the operational numerical weather prediction model of the Norwegian Meteorological Institute to simulate several observed cases of polar lows near Scandinavia. In those cases in which sensitivity studies were carried out, the absence of surface fluxes led to somewhat weaker cyclones, though usually some disturbance developed, presumably through (moist) baroclinic instability.

There is evidently more than one mechanism operating to produce the spectrum of phenomena called polar lows, although one mechanism may dominate the other in a particular circumstance. One of these mechanisms is certainly baroclinic instability while the other(s) involve CISK or air–sea interaction. The authors have recently argued against CISK as a mechanism for tropical cyclogenesis (Emanuel, 1986; Rotunno and Emanuel, 1987). In the first place, when viewed in the proper thermodynamic framework, the tropical atmosphere is very nearly neutral to deep moist convection (Betts, 1982), presumably being maintained in the convectively adjusted state by convection itself. The reservoir of available potential energy assumed by Charney and Eliassen (1964) and Ooyama (1964) in their original concept of CISK apparently does not exist in the tropical atmosphere. Secondly, tropical cyclones can be maintained in intense steady states without ambient conditional instability (Emanuel, 1986) and can intensify under the same conditions, provided a starting disturbance of sufficient amplitude exists (Rotunno and Emanuel, 1987). The finite-amplitude nature of the tropical cyclone viewed as an air–sea interaction instability is in good accord with the observation that tropical cyclones always arise from pre-existing disturbances such as easterly waves; this contrasts with the linear nature of CISK.

It seems likely that the convection observed in the environment of polar lows similarly serves to maintain a nearly moist adiabatic lapse rate, with no substantial stored convective available potential energy. Soundings near polar lows confirm this supposition (Shapiro et al., 1987). At the same time, the saturation moist entropy of the sea surface may be considerably higher than that of the atmosphere, as in the tropics, though in the case of the polar low environment much of this is due to an actual sea–air temperature difference. These observations lead us to ask whether hurricanes might be possible over the polar oceans in winter. In the following section, we extend the steady-state theory of Emanuel (1986) to account for sensible as well as latent heat input from the sea and calculate the minimum sustainable central pressure of polar lows resulting purely from air–sea interaction. We use a polar low proximity sounding to estimate the central pressure of an observed low and compare this estimate with observations in Section 3. In Section 4 we present the results of numerical experiments using the nonhydrostatic axisymmetric model of Rotunno and Emanuel (1987). A discussion of these results and inferences regarding the role of other processes such as baroclinic instability are presented in Section 5.

2. The maximum sustainable pressure drop due to sea–air heat flux

The gradient of pressure between the core and exterior of a cyclone represents a reservoir of potential energy. Bernoulli's equation may be used to show that in a steady circulation, the total pressure drop balances frictional dissipation in the boundary layer. Following a streamline near the sea surface from the outermost closed isobar of a circulation into the storm center, Bernoulli's equation may be written

$$\int_{r_0}^{0}\left[\mathrm{d}\left(\frac{1}{2}V^2\right)+\alpha\,\mathrm{d}p+g\,\mathrm{d}z-\boldsymbol{F}\cdot\mathrm{d}\boldsymbol{l}\right]=0, \qquad (1)$$

where V is the magnitude of the velocity, α the specific volume, p the pressure and $\boldsymbol{F}$ is the frictional force per unit mass. Since, by definition, we take $V=0$ at the outer radius r_0 and

since V also vanishes at $r = 0$, the above reduces to

$$\int_{r_0}^{0} \alpha \, dp = \int_{r_0}^{0} \boldsymbol{F} \cdot d\boldsymbol{l}. \tag{2}$$

The validity of the above does not depend on any assumption to the effect that boundary layer air actually penetrates all the way into the center. For example, the air may actually flow outward from the center to the eyewall and there meet up with inflowing air. Since pressure and velocity must be continuous at the radius where the two streams meet, (1) and (2) are still valid.

Emanuel (1986) showed how Carnot's theorem can be used to find the boundary layer frictional dissipation in (2). This was done by assuming that the mechanical energy generated by the Carnot cycle is used in the steady state to balance dissipation in the boundary layer and at large radii in the outflow, where an exchange of angular momentum must take place to allow the outflow to match the environment. This treatment has been extended by Emanuel (1988) to account for fully reversible thermodynamics. The estimate of central pressure thus obtained depends only on the assumptions of steadiness and small dissipation except in the aforementioned regions. (An assumption of axisymmetry is necessary only to estimate work done by the outflow, which was shown by Emanuel (1986) to usually be small compared to boundary layer dissipation.) Here we wish to further generalize the development by accounting for sensible as well as latent heat flux from the sea surface. It is possible to formulate an exact expression for minimum sustainable pressure following along the lines of Emanuel (1988), but for the sake of brevity we present a simplified treatment here. In this simplification, we neglect the effects of water substance on density and the work done against friction in the outflow. The former should be a good approximation at the low temperatures in which polar lows form, while the latter is valid in proportion to the smallness of the storm diameter (Emanuel, 1986). These two approximations have opposing effects on the central pressure estimate.

Consider a cross-section through a hypothetically steady polar low as shown in Fig. 1. Follow a parcel inward along the sea surface from which it extracts sensible and latent heat. The parcel then rises through the system, conserving its moist entropy, flows out to large radius, and descends while losing entropy through radiation to space. To close the cycle, the parcel eventually returns to the surface with its original moist entropy. While the last leg of the cycle is somewhat artificial, it is not necessary to view the parcel as actually following a closed cycle, since Bernoulli's equation is also valid when integrated along a vortex line, which in this case corresponds to an angular momentum surface.

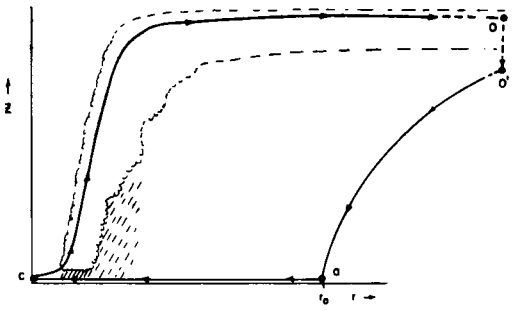

Fig. 1. The integral path for the Carnot cycle. Points o and o′ are taken to lie at very large radius.

The Carnot theorem can be easily derived from (1) and the first law of thermodynamics. If (1) is integrated around the whole circuit in Fig. 1, the result is

$$\oint \alpha \, dp = \oint \boldsymbol{F} \cdot d\boldsymbol{l}. \tag{3}$$

Neglecting effects of water substance on heat capacity and density, the first law of thermodynamics may be written (see the Appendix):

$$T \, ds = C_{pd} \, dT + L_v \, dw - \alpha \, dp, \tag{4}$$

where s is the moist entropy for saturated or unsaturated air, C_{pd} the heat capacity of dry air at constant pressure, L_v the heat of vaporization (or sublimation, if the phase change is between vapor and ice) and w is the vapor mixing ratio. Eliminating $\oint \alpha \, dp$ between (4) and (3) gives

$$\oint T \, ds = -\oint \boldsymbol{F} \cdot d\boldsymbol{l}, \tag{5}$$

which is Carnot's statement that the total heat input must balance frictional dissipation in a steady heat engine.

Under the simplifying assumption that all dissipation occurs in the boundary layer, (5) reduces to

$$\oint T\,ds = -\int_a^c \boldsymbol{F}\cdot d\boldsymbol{l}. \tag{6}$$

Since moist entropy is gained from the surface and lost between points (o) and (a) in Fig. 1, (6) can be written

$$\int_a^c T\,ds - T_{out}(s_c - s_a) = -\int_a^c \boldsymbol{F}\cdot d\boldsymbol{l}, \tag{7}$$

where T_{out} is an entropy-weighted mean outflow temperature:

$$T_{out} \equiv \frac{1}{s_c - s_a}\int_c^a T\,ds. \tag{8}$$

If we now use (2) to eliminate the frictional dissipation in (7), the result is

$$\int_a^c T\,ds - T_{out}(s_c - s_a) = -\int_a^c \alpha\,dp. \tag{9}$$

Finally, we once again use (4) to eliminate $\int_a^c \alpha\,dp$ from (9), arriving at

$$T_{out}(s_c - s_a) = C_{pd}(T_c - T_a) + (L_v w)_c - (L_v w)_a, \tag{10}$$

where the subscripts c and a denote evaluation at the low center and in the ambient environment, respectively.

As derived in the Appendix, an expression for moist entropy valid for both saturated and unsaturated air is:

$$s = (C_{pd} + C_\ell Q)\ln T + \frac{L_v w}{T} - R_d \ln p_d - wR_v \ln \mathrm{RH}, \tag{11}$$

where C_ℓ is the heat capacity of liquid water, Q is the total water content, p_d the partial pressure of dry air, R_v the gas constant for water vapor and RH is the relative humidity. Consistent with our previous neglect of the effects of water substance on density and heat capacity, we neglect C_ℓ and the difference between p_d and p in (11) as well as the temperature dependence of L_v in (10) and (11). Consistency also requires us to neglect the variability of temperature in the denominator of the term $L_v w/T$ and the last term on the right-hand side of (11) (see the Appendix). Substituting (11) into (10), with these approximations, we obtain

$$T_{out}\left(C_{pd}\ln\frac{T_c}{T_a} + \frac{L_v(w_c - w_a)}{T_c} - R_d \ln\frac{p_c}{p_a}\right) = C_{pd}(T_c - T_a) + L_v(w_c - w_a). \tag{12}$$

For convenience, we define a thermodynamic efficiency, ε:

$$\varepsilon \equiv \frac{T_c - T_{out}}{T_c}, \tag{13}$$

and we assume that the temperature difference $T_c - T_a$ is small enough that

$$\ln\frac{T_c}{T_a} \simeq \frac{T_c - T_a}{T_c}.$$

Using these and $w \simeq (R_d/R_v)e/p$ (where e is the vapor pressure), (12) can be written

$$\ln x = -\frac{A}{x} - B, \tag{14}$$

where

$$x \equiv \frac{p_c}{p_a},$$

$$A \equiv \frac{e_c}{p_a}\left[\frac{\varepsilon}{1-\varepsilon}\frac{L_v}{R_v T_c}\right],$$

$$B \equiv \frac{T_c - T_a}{T_c}\left[\frac{\varepsilon}{1-\varepsilon}\frac{C_{pd}}{R_d}\right] - \frac{e_a}{p_a}\left[\frac{\varepsilon}{1-\varepsilon}\frac{L_v}{R_v T_c}\right].$$

The term A/x in (14) reflects the pressure dependence of the water vapor mixing ratio while the first term in B above represents part of the sensible heat input from the ocean. The sum of A/x and the last term in B is the latent heat input.

The expression (14) yields the central pressure of a cyclone maintained entirely by surface heat fluxes, given the central surface air temperature and relative humidity as well as those quantities evaluated in the ambient environment, and the entropy-weighted mean outflow temperature as defined by (8). While (14) is implicit for the ratio $p_c/p_a (\equiv x)$, it is easily solved iteratively. (Emanuel, 1988, showed that (14) has no solutions under certain conditions, but this will not be a problem in the present investigation.) The maximum sustainable pressure drop is obtained by setting T_c equal to the sea surface temperature and $\mathrm{RH}_c = 1$.

3. Comparison with observations of a polar low

A beautiful example of a polar low that occurred in the Barents Sea north of Norway has been described by Rasmussen (1985). This case is particularly suited to comparison with theory since its environment was sampled by rawinsonde observations within 200 km of the low center and since ship observations were made very close to the low center. The cyclone was typical of polar lows near Scandinavia, with a clear eye surrounded by deep convective clouds. Like many polar lows, this one formed near the center of a deep cut-off cyclone aloft.

The surface analysis at 0000 GMT on 14 December 1982 is reproduced in Fig. 2. The cyclone apparently formed 24–36 hours preceding this time somewhere just southwest of Bear Island (the station reporting a temperature of −8°C and dewpoint of −9°C). Satellite imagery presented by Rasmussen (1985) shows that the clear central eye had become less well defined by this time, but the central pressure was well known due to the proximity of a ship. The polar low formed in a region of generally low surface pressure associated with the cyclones at the eastern edge of the map. The ship near the polar low center is reporting a south wind of 20 $m s^{-1}$, a pressure of 980.2 mb and snow showers. Its temperature (0°C) and dewpoint (−1°C) are significantly higher than those of surrounding stations. If we assume that the wind field is in solid body rotation between the location of the

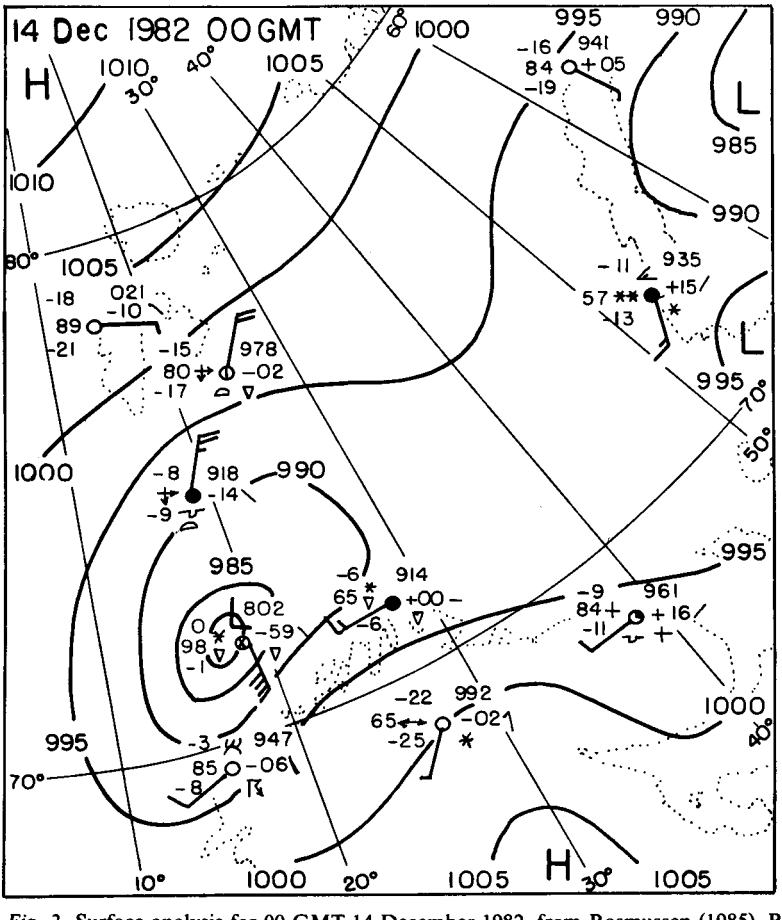

Fig. 2. Surface analysis for 00 GMT 14 December 1982, from Rasmussen (1985). Bear Island is near 75°N, 19°E reporting a temperature of −8°C.

ship and the storm center, then cyclostrophic balance gives a central pressure of 975–980 mb (independent of the distance between the storm center and the ship).

The Carnot cycle theorem developed in the previous section gives the pressure change between the storm center and the outermost closed isobar, where the air is considered to begin its inward movement toward the center. Because the polar low in this case formed in a region of substantial ambient pressure gradient, an unambiguous estimate of the outer pressure is not possible. Based on the analysis shown in Fig. 2 and on surface analyses over the preceding 24 hours, we take the outer pressure to be 993 mb.

The Bear Island sounding taken 12 hours before the analysis time of Fig. 2 is reproduced in Fig. 3. At this time, satellite imagery (see Rasmussen, 1985) shows a clear central eye about 75 km in diameter located roughly halfway between Bear Island and the northern Norwegian coast. The Bear Island sounding was taken just inside the northern limit of the cloud shield associated with the polar low.

The sounding in Fig. 3 exhibits a nearly moist adiabatic temperature lapse rate between 830 mb and the tropopause at 410 mb, perhaps reflecting moist adiabatic adjustment by deep cumulonimbi a short distance south over the open ocean. A nearly isothermal layer extends from the surface to 830 mb, reflecting arctic air that has travelled southward over ice. Bear Island is located at the southern extremity of the sea ice at this time.

Two obvious difficulties in using this or any other sounding as a reflection of the polar low environment are that the sounding is apt to be changing in time, even away from the cyclone, and the environment varies spatially as one moves around the perimeter of the disturbance. In this particular case, the polar low occurred near (but not necessarily at) the center of a deep cut-off low aloft so that the temperature does not vary much in the horizontal above about 800 mb. But, as is clear in Fig. 2, a large north–south temperature gradient exists near the surface in association with the ice edge.

The structure of the Bear Island sounding does suggest, on the other hand, that most of the temporal and spatial variability of the atmospheric thermodynamic structure in the environment of the polar low will occur below 830 mb.

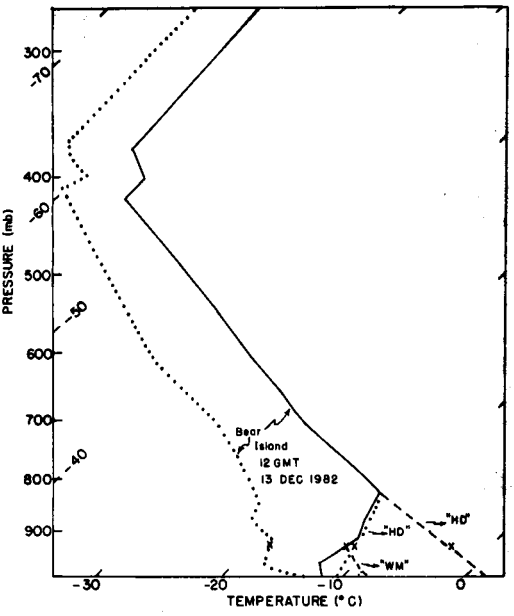

Fig. 3. Bear Island sounding at 12 GMT 13 December 1982. (See Fig. 2 for location of Bear Island.) Solid lines show temperature sounding; dotted lines are dew point temperature. The modifications HD and WM discussed in the text are shown by dashed lines (temperature) and dotted lines (dew point). CD is identical to the actual sounding. The quantities used at the lowest grid points of the numerical model are shown by × 's.

While surface heating can lead to rapid modification of the sounding below this level, once an adiabatic lapse rate is established from 830 mb downward, further surface heating will lead to turbulent fluxes over a much deeper layer (essentially the whole troposphere) with a correspondingly much slower change in temperature and moisture. Inspection of Figs. 2 and 3 reveals that the only surface air that is capable of rising buoyantly above 830 mb is air very close to the polar low center. We therefore feel confident in assuming that the Bear Island sounding (Fig. 3) accurately reflects the polar low environment above 830 mb.

Our strategy for dealing with the environment below 830 mb is simply to perform three separate calculations based on three assumptions about the environment at low levels. These are described as follows.

(1) Cold and Dry ("CD"). This assumes that

the low-level environment is that of the Bear Island soundings shown in Fig. 3. Since this is probably the coldest air at that distance from the low center, this represents an extreme estimate on the cold side.

(2) Warm, Moist ("WM"). Here we assume that the surface air has the temperature and dewpoint (−8°C, −9°C) of Bear Island at the analysis time of Fig. 2, and that the sounding is adiabatic from the surface upward to the point at which the relevant moist adiabat intersects the 12 GMT Bear Island sounding. This represents our "best estimate" of the low-level environment at 0000 GMT 14 December.

(3) Hot, Dry ("HD"). Here we take the lower atmosphere to be dry adiabatic from the 830 mb level (Fig. 3) down to the surface, with a lifting condensation level of 830 mb. This represents an extreme estimate on the warm side. These modifications are shown in Fig. 3.

Each of these soundings yields the environmental estimates needed to calculate central pressure using (14). The central temperature and vapor pressure are taken from the 0000 GMT AMI ship observation near the low center (Fig. 2) which recorded a temperature of 0°C and dewpoint of −1°C. (A continuous time series of temperature from ship AMI actually shows that the temperature increased to nearly 1°C as the cyclone passed the ship (see Rasmussen, 1985) but the dewpoint fell to −2°C indicating almost no change in θ_e.)

Calculation of the thermodynamic efficiency, ε, requires knowledge of the mean outflow temperature defined by (8). This is estimated, as in Emanuel (1986), by assuming that air flows out of the low at its level of neutral buoyancy with respect to the environment. To calculate T_{out} defined by (8), we begin by lifting *ambient* surface air to its level of neutral buoyancy (which may be at the surface) and finding the temperature at that level. Then the θ_e of the surface air is increased by a small increment (we choose 2°C) and the new temperature at the new neutral buoyancy level is found. This procedure is repeated until we achieve the observed θ_e of the air at the low center. The resulting temperatures are then averaged to find T_{out} and thus ε, as defined by (13).

Clearly, the smallest estimate of ε will occur in sounding CD due to the small value of surface θ_e, while the largest will obtain from HD. On the other hand, the greatest difference between ambient and central temperature and vapor pressure will occur in sounding CD. These effects tend to cancel each other in the calculation of central pressure using (14).

Estimates of the central pressure made from the three soundings are listed in Table 1, assuming an ambient pressure of 993 mb. The estimates made using sounding WM and HD are very close to the observed central pressure of about 978 mb, although the estimate from sounding CD is not far off. It is evident that the difference in soundings at low levels has a noticeable, but not large, effect on the storm's intensity. The good agreement between the estimates of central pressure made using (14) and observations suggests, but does not entirely prove that surface sensible and latent heat fluxes were instrumental in the development of this polar low. It could be argued that the high temperature and water vapor content near the low center were the result of horizontal advection, as in a purely baroclinic disturbance, but inspection of Fig. 2 and previous surface analyses (Rasmussen, 1985) shows that no air with similar values of θ_e could be found in the environment (though a tongue of high θ_e air may have slipped between the surface observations).

The last entry in Table 1 shows the central pressure that would have resulted if the air near

Table 1. *Estimates of central pressure from eq. (14) for three environmental soundings (see text); assumed ambient pressure is 993 mb*

Sounding	T_c (°C)	e_c (mb)	T_a (°C)	e_a (mb)	ε	p_c (mb)
CD	0	5.68	−12	2.45	0.0788	974
WM	0	5.68	−8	3.10	0.0912	978
HD	0	5.68	0	3.10	0.2123	979
. . . . .						
WM	7	10.01	−8	3.10	0.181	922
						918*

$T_c \equiv$ central surface air temperature.
$T_a \equiv$ ambient surface air temperature.
$e_c \equiv$ central surface vapor pressure.
$e_a \equiv$ ambient surface vapor pressure.
* Calculated using latent heat of sublimation. Values of p_c estimated above are the same to within 1 mb when heat of sublimation is used.

the polar low center had warmed up to and become saturated at the observed sea surface temperature of about 7°C. This represents the minimum sustainable pressure permitted by the Carnot cycle mechanism. Its value of 922 mb is similar to minimum sustainable pressure estimates of tropical hurricanes. This shows that the thermodynamic potential for hurricanes is large in the polar low environment although, to be sure, the kinematic structure of the ambient environment is very different from that observed in hurricane genesis regions. We will show, in Section 3, that this might be an important difference. Since polar lows in this region typically spend less than 2 days over relatively warm water it is not surprising that their central pressures do not approach the minimum value allowed by the Carnot cycle.

It is a straightforward matter to calculate the relative magnitudes of the sensible and latent heat input from the ocean for each of the ambient soundings listed in Table 1 and using the ship observations for thermodynamic data near the low center. The ratios of sensible to latent heat input for soundings CD and WM are 2.6 and 2.2, respectively, showing that the sensible heating is dominant. The ratio for sounding "HD" is 0.3 with all the sensible heating due to isothermal expansion. For the minimum sustainable pressure calculation, the sensible-to-latent heat ratio is 1.7.

The thermodynamic calculations presented here demonstrate that sea–air heat fluxes can indeed account for much of the energetics of polar lows. In the following section we explore the dynamics of polar lows resulting from air–sea interaction.

4. Numerical simulations

In designing numerical experiments suitable for examining the extent to which polar lows can develop through air–sea interaction, it is desirable to exclude other physical processes that might lead to cyclogenesis. For this purpose, we employ a tropical cyclone model whose axisymmetry precludes the operation of baroclinic or barotropic instability. We use the model described by Rotunno and Emanuel (1987). Briefly, the model integrates the nonhydrostatic primitive equations expressed in a cylindrical coordinate system with uniform grid spacing in the radial and vertical directions. The model equations consist of conservation laws for momentum, mass, heat, water vapor and liquid water. The microphysical scheme differs from that used in hurricane simulations in that all condensed water is assumed to be in the form of snow. As a result, we add the latent heat of sublimation and permit no evaporation. Condensate in excess of 1 $g kg^{-1}$ is taken to fall at a constant terminal velocity of 1 $m s^{-1}$. The turbulence scheme employs an eddy viscosity which depends on the local rate of deformation and Richardson number. Surface fluxes are represented by bulk aerodynamic formulae with wind-dependent exchange coefficients. A sponge layer placed in the stratosphere well above the region containing the main circulation controls gravity wave reflections there while a wave radiation condition at the outer boundary minimizes the amplitude of reflected waves. Radiation is neglected. Moist convection is explicitly, albeit crudely, simulated by the model. Particular values of the parameters used in the simulations are listed in Table 2.

In estimating the initial thermodynamic environment we once again assume that the Bear Island sounding shown in Fig. 3 is representative of the polar low environment above 830 mb and perform three separate experiments corresponding to the soundings WM, HD and CD. The

Table 2. *Model parameters*

Parameter	Value	Description
l_0	200 m	mixing length
l_H	2000 m	horizontal mixing length
V	1 $m s^{-1}$	terminal velocity of frozen water ($=0$ if $q_r < 1$ $g kg^{-1}$)
τ_R	∞	no radiative damping
c^*	30 $m s^{-1}$	wave speed for open boundary condition
Z_{sponge}	12.5 km	bottom of "sponge" layer
α_{max}	0.013 s^{-1}	maximum value of damping in "sponge" layer
Z_{top}	15 km	domain top
r_{outer}	1500 km	domain outer radius
ΔZ	1 km	vertical grid size
Δr	10 km	horizontal grid size
Δt	20 s	time step
f	0.000136 s^{-1}	Coriolis parameter at 70°N latitude

differences between these soundings affect only the lowest thermodynamic grid points in the model; these modifications are shown in Fig. 3.

4.1. *Experiments with no flow aloft*

In the first set of experiments we begin with a kinematic environment similar to that associated with hurricane formation; that is, with no substantial flow aloft. In Subsection 4.2 we will examine the effects of an initial cold-core cyclone in the upper troposphere.

As a starting vortex we specify an azimuthal wind field of the form

$$V = V_s F_s(r) \begin{cases} \left(1 - \dfrac{z}{z_t}\right) & \text{for } z \leqslant z_t \\ \dfrac{H}{z_t}\left(1 - \dfrac{z}{H}\right)\left(\dfrac{z_t - z}{H - z_t}\right) & \text{for } z > z_t, \end{cases} \tag{15}$$

where

$$F_s(r) \equiv \frac{2r/r_{max}}{1 + (r/r_{max})^2}.$$

The temperature field is then determined by integrating the thermal wind equation outward from the center where the temperature is specified as discussed above. The initial circulation thus consists of a warm core vortex with maximum wind V_s occurring at the surface at a radius of r_{max} and decaying linearly with height to zero at $z = z_t$. The part of the flow above z_t is designed so that $\partial V/\partial z$ (and thus $\partial\theta/\partial x$) is continuous across z_t and such that V vanishes at $z = H$. In practice it results in a weak anticyclonic flow between z_t and H.

In a "control" experiment, hereafter denoted "A", we use sounding WM and set $V_s = 10\ \mathrm{m\,s^{-1}}$, $r_{max} = 50$ km, and $z_t = 6.5$ km. The time evolution of the maximum azimuthal wind is shown in Fig. 4. After an initial period of adjustment the cyclone intensifies from about 8 $\mathrm{m\,s^{-1}}$ to hurricane force during the 24-h period beginning 10 h after initialization. Also shown in Fig. 4 is the evolution of maximum wind for two experiments identical to A but using soundings HD and CD (denoted experiments B and C, respectively). As in the steady state theory, there is little difference in the final intensity of the storms.

The structure of the mature stage of the cyclone of experiment A is highlighted in Fig. 5

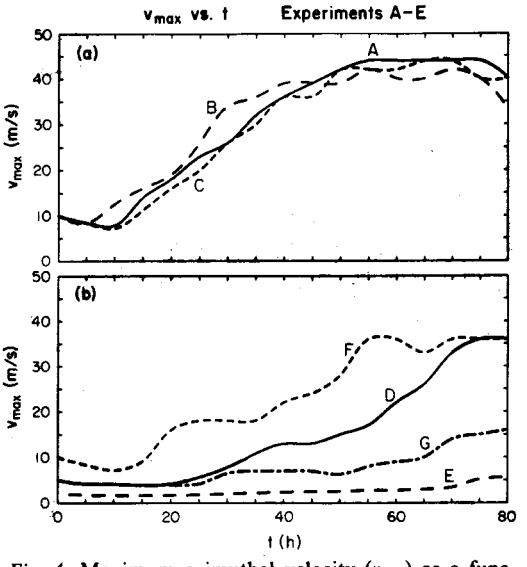

Fig. 4. Maximum azimuthal velocity (v_{max}) as a function of time for experiments A–C (a) and D–G (b).

which shows various fields averaged over the period between 80 and 90 h after initialization. The fields bear a strong resemblance to those characteristic of hurricanes except that the circulation is shallower and the thermal structure shows a warm ring near the surface in addition to the warm core aloft. The former arises as a consequence of the strong sensible heat transfer from the sea surface which is absent in true hurricanes. As a result of this warm ring structure, the azimuthal velocity contours slope inwards at low levels near the center. The condensate distribution reveals a ring of deep convection surrounding a clear central eye with considerable convective activity extending out to large radii. The θ_e field (Fig. 5g) bears a strong resemblance to the θ_e cross-sections through the polar lows that appear in the mesoscale numerical simulations described by Grønås et al. (1987) and Nordeng (1987).

As in our earlier simulations of hurricanes, the development of polar lows in our model is sensitive to the amplitude and geometric size of the starting vortex. We performed a number of experiments in which the size and amplitude of the initial vortex are varied; these are summarized in Table 3 and the evolution of the velocity maximum with time is shown in Fig. 4b. In

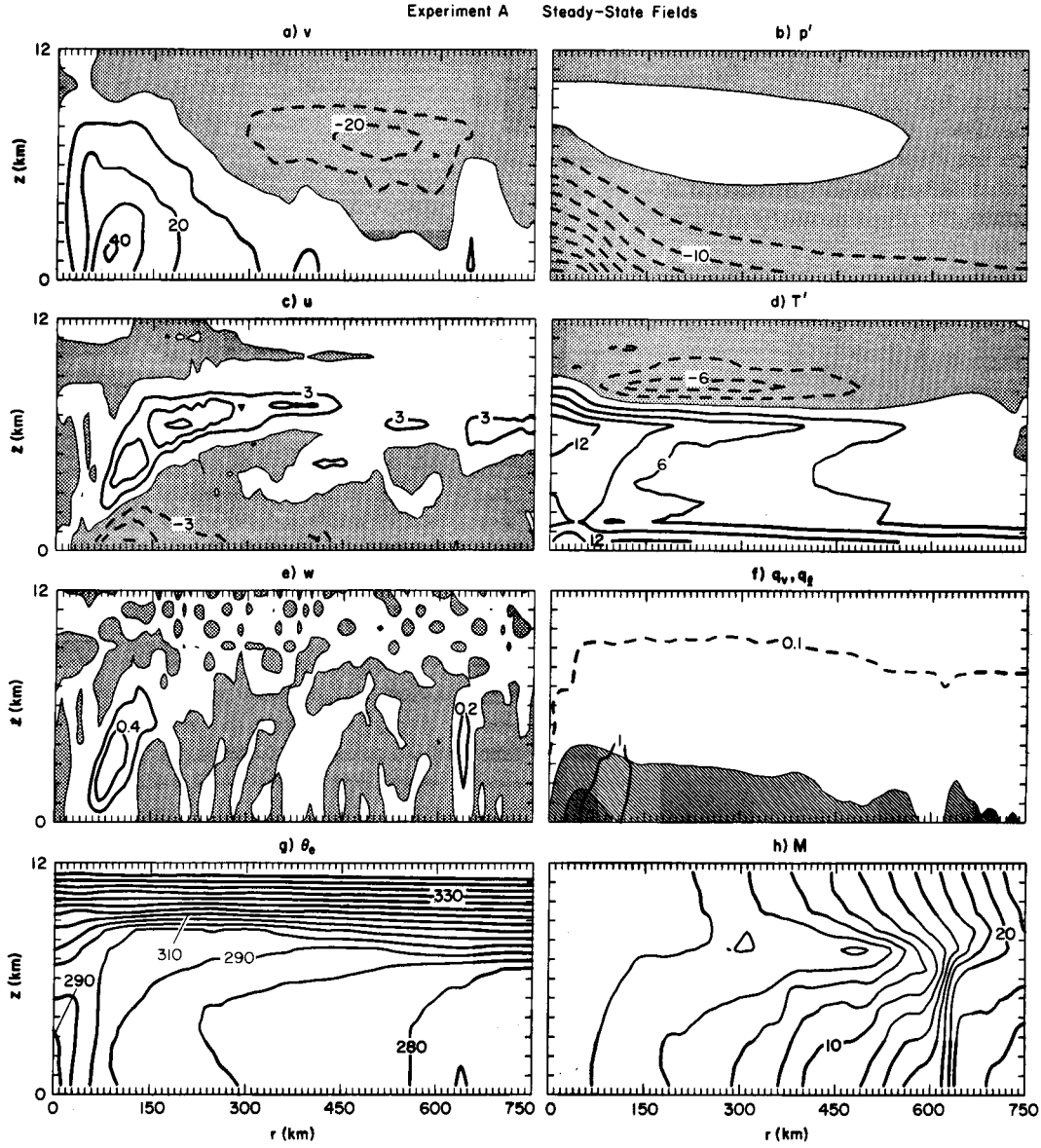

Fig. 5. The 80–90 h average fields for the nearly steady state reached by the control run (experiment A). All stippled regions indicate negative values of the fields. (a) Azimuthal velocity, contour interval 10 ms^{-1}; (b) pressure deviation from initial state, contour interval 5 mb; (c) radial velocity, contour interval 3 ms^{-1}; (d) temperature perturbation from initial state, contour interval 3 C; (e) vertical velocity, contour interval 0.2 ms^{-1}; (f) water vapor mixing ratio (q_v) and snow mixing ratio (q_l). Light shading denotes $1 < q_v < 3$ gkg^{-1}, dark shading indicates $q_v > 3$ gkg^{-1}. Snow contours are 0.1 gkg^{-1} (dashed) and 1 gkg^{-1} (solid); (g) equivalent potential temperature, contour interval 5°C; (h) angular momentum in dimensionless units such that $M\,[r = r_{outer}] = 100$, contour interval 2.

Table 3. *Initial conditions used in the numerical experiments*

Experiment	r_{max} (km)	V_s (ms^{-1})	r_m (km)	V_m (ms^{-1})	Sounding
A	50	10		0	WM
B	50	10		0	HD
C	50	10		0	CD
D	50	5		0	WM
E	50	2		0	WM
F	100	10		0	WM
G	100	5		0	WM
H	50	10	500	20	WM
I	100	10	500	20	WM
J	50	5	500	20	WM

$r_{max} \equiv$ radius of maximum surface winds.
$V_s \equiv$ maximum surface winds.
$r_m \equiv$ radius of maximum winds at tropopause.
$V_m \equiv$ maximum winds at tropopause.

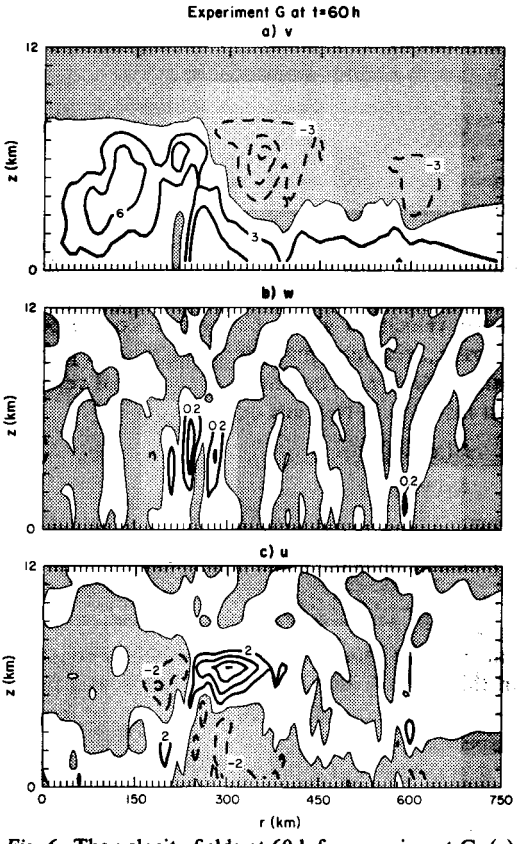

Fig. 6. The velocity fields at 60 h for experiment G. (a) Azimuthal velocity, contour interval 3 ms^{-1}; (b) vertical velocity, contour interval 0.2 ms^{-1}; (c) radial velocity, contour interval 2 ms^{-1}. Stippling indicates negative values.

experiments D and E, the maximum velocity of the initial vortex is reduced to 5 and 2 ms^{-1}, respectively. The former intensified to an amplitude similar to that reached by A, whereas the latter did not amplify significantly. For this initial vortex size, the "critical amplitude" lies somewhere between 2 and 5 ms^{-1}. The sensitivity to initial amplitude is restricted to a determination of whether or not there is amplification; given an initial vortex of sufficient intensity, there will be amplification to a quasi-steady state which is not itself sensitive to the magnitude of the starting vortex.

Experiments F and G begin with a vortex whose radius of maximum winds lies at 100 km. When the initial amplitude is 10 ms^{-1} (experiment F), the cyclone intensifies to almost the magnitude of the control experiment, whereas experiment G, beginning with half the amplitude of F, does not intensify to the extent of F. Closer inspection of the velocity fields of experiment G reveals that the surface winds hardly increase at all; the increase of velocity shown in Fig. 4 occurs in the upper part of the vortex (see Fig. 6). Apparently, the ring of convection develops at a larger radius and, as a consequence, the inward branch of the outflow aloft spins up a vortex inside the ring of convection at higher levels. The energy available from the Carnot cycle is used up in amplifying the circulation aloft, which does not have any feedback on the surface fluxes. This can be better understood by examining the response of the circulation in the $r-z$ plane to a specified heat source, using the Boussinesq form of the Sawyer–Eliassen equation in cylindrical coordinates:

$$\frac{1}{r^3}\frac{\partial M^2}{\partial r}\frac{1}{r}\frac{\partial^2 \psi}{\partial z^2} + N^2 \frac{\partial}{\partial r}\left(\frac{1}{r}\frac{\partial \psi}{\partial r}\right) = \frac{\partial Q}{\partial r}, \qquad (16)$$

where Q is proportional to the heating, N is the buoyancy frequency (assumed constant), ψ is the streamfunction in the $r-z$ plane, and M is the angular momentum per unit mass, defined as

$$M \equiv rV + \tfrac{1}{2} fr^2,$$

where f is the Coriolis parameter. For simplicity, we examine solutions to the above for the case

that V is a linear function of r (in which case $(1/r^3)\partial M^2/\partial r$ is a constant), and Q is a delta function in r and is sinusoidal in z:

$$Q = Q_0 \delta(r, r_0) \sin \frac{\pi z}{H}, \tag{17}$$

where Q_0 is a constant, H is the depth of the circulation, and r_0 is the radius at which the heating is applied. Analytic solutions can be obtained for this system in terms of Bessel functions. Of particular interest is the distribution of radial velocity u which changes discontinuously across r_0, reaching maximum magnitudes just on either side of r_0. The ratio β of the radial velocity just inside r_0 to that just outside r_0 is

$$\beta = \frac{I_1(x) K_0(x)}{K_1(x) I_0(x)}, \tag{18}$$

where x is the ratio of r_0 to the deformation radius:

$$x \equiv r_0 \frac{\pi \eta}{NH},$$

and η is the absolute vorticity which is constant in this case. I_n and K_n are modified Bessel functions of order n of the first and second kinds, respectively.

A graph of β as a function of x is displayed in Fig. 7. For x less than about 0.3, the radial velocities inside the ring of heating are negligible compared with those outside the heating maximum. Since the spin up of a constant vorticity vortex is directly proportional to u we infer that for sufficiently small x most of the velocity changes will be outside the heating maximum. In the nonlinear regime the cyclonic velocities will always exceed the anticyclonic so that a ring of heating at small x will produce strong surface cyclonic flow and weak anticyclonic flow aloft, thus facilitating strong feedback through surface heat fluxes. If x is too large, however, the radial outflow aloft will spin up a relatively strong cyclone inside the heating maximum aloft and less energy will flow into the surface cyclone with correspondingly less feedback from surface fluxes. In the foregoing experiments, the effective Rossby radius, $NH/\pi\eta$, $\simeq (0.01\ \text{s}^{-1})(6500\ \text{m})/\pi(1.36 \times 10^{-4}\ \text{s}^{-1}) \approx 230$ km. Since the initial heating is near r_{max}, we infer that $x \approx 0.22$ in the control run. In experiment G, however, $x \approx 0.44$ initially and, as is evident from Fig. 6, expands to $x \approx 1.0$, which is a decidedly unfavorable situation. We believe that this is the reason that initial vortices with large radii of maximum winds do not amplify. This also might explain why polar lows generally have smaller diameters than hurricanes, since the Coriolis parameter is larger and thus x will be larger for a given radius.

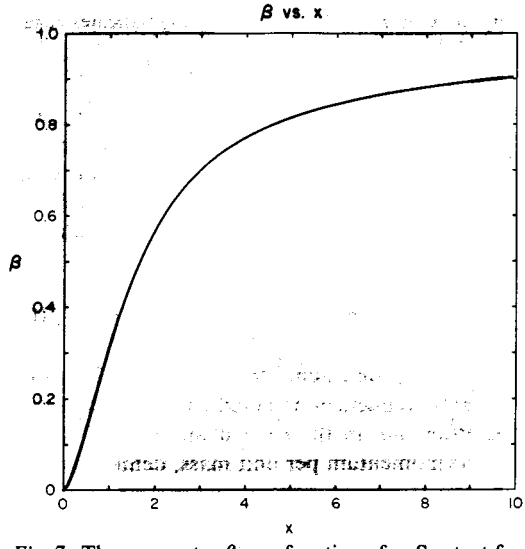

Fig. 7. The parameter β as a function of x. See text for explanation.

The time-scale of development of disturbances in the model is sensitive to the magnitude of the surface exchange coefficients. A reviewer has pointed out that the use of Deacon's formula, which was developed principally for the tropics, may seriously underestimate the fluxes in the highly unstable boundary layers typical of the polar low environment. We therefore made an attempt to incorporate more realistic formulations of surface fluxes that include the wind-dependence of the surface roughness length and the bulk stability. A review of the literature on this subject unfortunately reveals a wide spectrum of results; there does not even appear to be agreement on whether the surface exchange coefficients for heat and moisture increase or decrease with wind speed. We did attempt to use the formulation of Louis (1979) to calculate the surface exchange coefficients of heat and momentum as a function of the bulk Richardson number and surface roughness length, the latter of which was estimated using Charnock's relation with a coefficient of 0.032. We found, rather

remarkably, that the results were very similar to those given by Deacon's formula. At high wind speeds, the Richardson number is small and the wind-dependence of the surface roughness yields results similar to Deacon's formula. At small wind speeds, the Richardson number is large but the surface roughness is small and again the dependence on wind speed is close to that given by Deacon. Moreover, all the coefficients were reasonably close to those measured by Large and Pond (1982) under unstable conditions.

We are discomfitted by the foregoing. Measurements of surface fluxes under the highly disequilibrated sea states and thermodynamic states typically accompanying polar lows are scarce and we feel that the actual exchange coefficients may be far larger than current formulations indicate. To investigate the sensitivity of the model to the exchange coefficients we simply doubled them. The result is that the model storm intensifies about 40% faster than the control run, though it reaches the same intensity. We also reran experiment E and found no significant difference up to 40 h; by 80 h some higher winds developed as convection broke out over a large area of the domain, but no coherent vortex circulation occurred.

4.2. *Experiments with an initial cold core cyclone aloft*

Observations of the type of polar low that we address in this study invariably show that they develop near or at the center of deep, cold core cut-off lows aloft (Businger, 1985). The particular polar low whose environment we specified for the numerical simulations discussed above was an example of one which developed nearly directly under an upper level cyclone (Rasmussen, 1985). Clearly, the cold air associated with such a system is favorable for the development of polar lows under our air–sea interaction hypothesis, but it is not clear what effects the circulations around a large scale cut-off low might have on the development of polar lows. In order to examine such effects, we have carried out several additional experiments in which we specify a cold-core upper cyclone in the initial condition. In particular, we add to the initial velocity field specified by (15) a cold core vortex of the form

$$V = V_m\left(\frac{z}{z_t}\right) f(r) \quad \text{for } z \leqslant z_t, \tag{19}$$

where V_m is the maximum velocity of the cold core cyclone and

$$f(r) = \frac{\alpha_p (r/\beta_p r_m)}{1 + (r/\beta_p r_m)^p},$$

where

$$\alpha_p \equiv \frac{p}{(p-1)^{1-1/p}},$$

and

$$\beta_p \equiv (p-1)^{1/p}.$$

This gives a vortex flow that decays rapidly with radius at large radius, but is always inertially stable. In the experiments to be described, we take $p = 5$. Once again, we specify a velocity field above $z = z_t$ such that $\partial v/\partial z$ is continuous across z_t and V vanishes at $z = H$:

$$V = V_m\left(\frac{H}{z_t}\right)\left(\frac{H-z}{H-z_t}\right)\left(1 + \frac{z_t}{H} - \left(\frac{H-z}{H-z_t}\right)\right) f(r) + V_s\left(\frac{H}{z_t}\right)\left(1 - \frac{z}{H}\right)\left(\frac{z_t - z}{H - z_t}\right) F_s(r) \quad \text{for } z > z_t. \tag{20}$$

The total initial velocity field is shown in Fig. 8 for the case $r_m = 500$ km, $V_m = 20$ m s^{-1}, $r_{max} = 50$ km, $V_s = 10$ m s^{-1}, $z_t = 6.5$ km and $H = 12.5$ km. Note that because of the imposed condition that $\partial V/\partial z$ be continuous, the actual velocity maximum is greater than V_m and occurs at a higher altitude.

We performed three experiments using different values of V_s and r_{max}; these are listed in Table 3 and the development of the *surface* velocity maxima with time is shown in Fig. 9. Experiment H is identical to the control run, A, except for the presence of the cold core vortex aloft in the initial condition. The cyclone develops to almost the

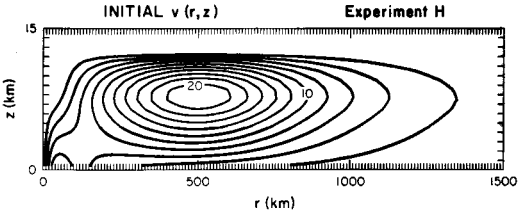

Fig. 8. Azimuthal velocity used as initial condition for experiment H. Contour interval 2 m s^{-1}.

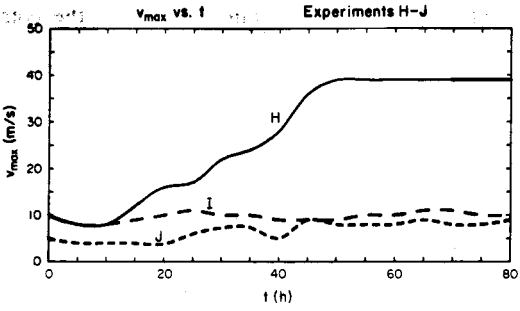

Fig. 9. Development of maximum azimuthal velocity at lowest grid points for experiments H–J.

same amplitude as A. The fields averaged between 80 and 90 h for experiment H are displayed in Fig. 10 and should be compared to those of A (Fig. 5). The surface cyclone is much more concentrated in the presence of the cut-off low aloft and the latter has been destroyed between about 90 and 170 km from the center. In this case, the upper cyclone does not appear to have inhibited development of the polar low. Inspection of Fig. 9 reveals, however, that the surface cyclone of experiment I, which is identical to F except for the cut-off low in the initial condition, does not develop at all, in contrast with F. Nor did experiment J which can be compared to D. Close inspection of the velocity fields in these cases (not shown) reveals that the lack of surface development appears to be for the same reasons we elaborated on in the case of experiment G; namely, that much of the energy available from the Carnot cycle flows into the development of a cyclone aloft, inside the convective ring, where it cannot feedback through the surface fluxes. This more readily occurs in the presence of an initial cyclone aloft because the deformation radius is smaller and thus x is larger for a given radius (see eq. (18) and Fig. 7). For this reason, the "critical" initial radius of maximum surface winds is smaller, and the critical velocity at fixed r_{max} larger when an upper level vortex is present initially.

5. Discussion

We have shown, in Section 3, that there is a certain thermodynamic similarity between polar air masses over relatively warm water and the tropical atmosphere in regions susceptible to hurricanes. In both cases, fluxes of sensible and/or latent heat from the underlying ocean surface can lead to substantial warming of a deep layer of the atmosphere. The particular environment of a polar low investigated by Rasmussen (1985) was shown to be capable of sustaining a pressure drop of up to 70 mb. Moreover, measurements of θ_e near the low center are consistent with the observed pressure drop.

Numerical simulations with an axisymmetric nonhydrostatic model show that air–sea interaction can produce cyclones whose structure is consistent with observations, but whose intensity is somewhat larger. The reasons for the different intensity are not clear, but several points come to mind. Sea surface temperatures near Norway (e.g., see Rasmussen (1985)) are relatively high only in a narrow tongue just west of the coast. The rapidly moving polar low simply may not remain over warm water long enough to achieve its potential intensity. The effect of the disturbances on the sea surface temperature is not known, but the strong winds and cyclonic circulation may induce enough mixing and upwelling to have a noticeable influence on the ocean temperature, as is observed with many tropical hurricanes. It is also true that only a few percent of all hurricanes intensify to the upper bound given by the Carnot theorem, but the reasons for this remain elusive.

We emphasize that, as in the case of tropical cyclones, the polar low environment appears to be stable to small amplitude axisymmetric perturbations; *disturbances of substantial amplitude are apparently necessary to initiate intensification by air–sea interaction.* To the extent that this is a valid finding, it points to the necessity of some presumably non-axisymmetric dynamical process that operates in the early stages of cyclogenesis. Baroclinic instability is one obvious candidate since baroclinicity is almost always present to some degree in the pre-cyclone environment. It is conceivable that the baroclinic mechanism operates cooperatively with air–sea interaction; if not, the development of polar lows might be thought of as a two-stage process. Other disturbances, such as topographically generated cyclones, might also act as starting disturbances. The nature of the amplitude conditions for growth by the air–sea interaction mechanism is

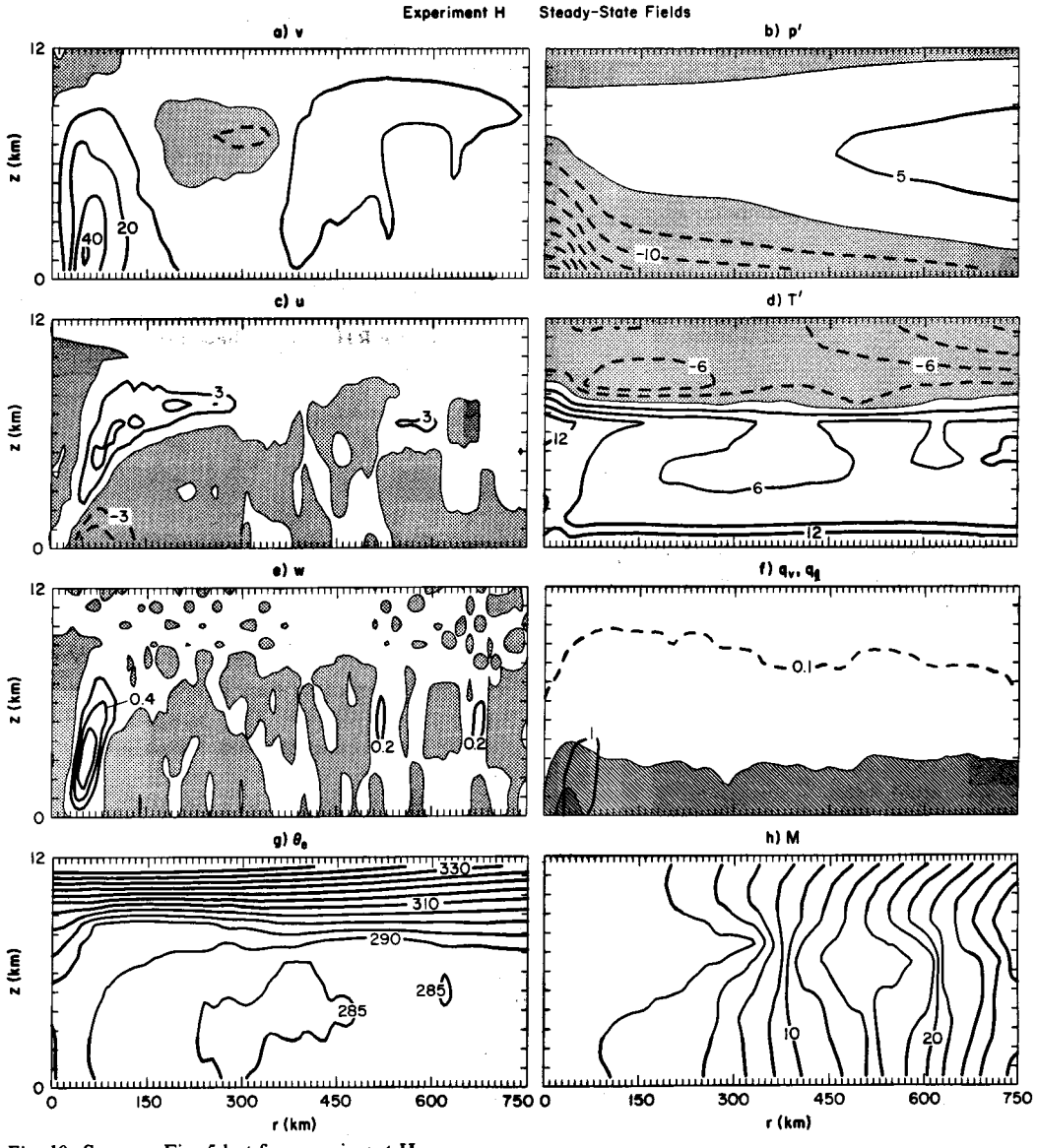

Fig. 10. Same as Fig. 5 but for experiment H.

the subject of on-going investigation by the authors.

Experiments with the numerical model show that the development of axisymmetric polar lows is sensitive to the initial kinematic as well as thermodynamic state of the atmosphere and to the formulation of the surface fluxes. In particular, the large inertial stability associated with cut-off lows aloft makes it necessary to start with a surface cyclone of higher amplitude and/or smaller radius of maximum winds; otherwise, the surface fluxes act to amplify the cyclone aloft rather than at the surface where it can feedback on the surface fluxes.

6. Acknowledgements

The contribution of Kerry Emanuel was supported by National Science Foundation Grant ATM-8513871 and the Office of Naval Research under contract N00014-87-K-0291. We should like to thank Joel Sloman for typing the manuscript and Isabelle Kole for drafting several of the figures.

7. Appendix

An expression for moist entropy valid in saturated and unsaturated air

The following quantity can be shown to be conserved during reversible moist or dry adiabatic expansion:

$$s = (C_{pd} + QC_\ell)\ln T + \frac{L_v w}{T} - R_d \ln p_d - wR_v \ln \mathrm{RH}, \qquad \text{(A1)}$$

where C_{pd} and C_ℓ are the heat capacities of dry air and liquid water, respectively, Q is the total water content, L_v is the heat of vaporization (a function of temperature), w the vapor mixing ratio, R_d and R_v are the gas constants for dry air and water vapor, respectively, and RH is the relative humidity.

Differentiation of (A1) yields

$$T\,ds = (C_{pd} + QC_\ell)\,dT + L_v\,dw - \frac{R_d T}{p_d}\,dp_d + w\,dL_v - \frac{L_v w}{T}\,dT - wR_v T\,d\ln \mathrm{RH} - R_v T \ln \mathrm{RH}\,dw. \qquad \text{(A2)}$$

The last term of (A2) vanishes since reversible changes in w can only occur at RH = 1. The temperature dependence of L_v is given by

$$dL_v = (C_{pv} - C_\ell)\,dT,$$

where C_{pv} is the heat capacity of water vapor at constant pressure. Also, the Clausius–Clapeyron equation may be written:

$$L_v \frac{dT}{T} = R_v T \frac{de_s}{e_s} = R_v T\left(\frac{de}{e} - \frac{d\mathrm{RH}}{\mathrm{RH}}\right),$$

since $e_s = e/\mathrm{RH}$. Using these two expressions in (A2) gives

$$T\,ds = (C_{pd} + wC_{pd} + \mathscr{C}_\ell)\,dT + L_v\,dw - \frac{R_d T}{p_d}\,dp_d - wR_v T \frac{de}{e}. \qquad \text{(A3)}$$

Finally, we note that since $w = \alpha_d/\alpha_v$, where α_d and α_v are the specific volumes of dry air and water vapor, respectively, (A3) can be written

$$T\,ds = (C_{pd} + wC_{pv} + \mathscr{C}_\ell)\,dT + L_v\,dw - \alpha_d\,dp, \qquad \text{(A4)}$$

which is a direct statement of the first law of thermodynamics written as entropy changes per unit mass of dry air. This proves that (A1) is a uniformly valid expression for entropy of moist air.

In the relatively cold environments of polar lows we neglect the effect of water substance on heat capacity and on density. If one follows through the derivation of (A4), it can be seen that consistency demands that we neglect the temperature dependence of L_v/T in the second term on the right of (A1), the last term in (A1), and the difference between p and p_d. Thus a consistent low temperature approximation to (A1) is

$$s \simeq C_{pd} \ln T + \frac{L_{v0}}{T_0} w - R_d \ln p, \qquad \text{(A5)}$$

where L_{v0} and T_0 are constants.

REFERENCES

Bergeron, T. 1954. Reviews of tropical hurricanes. *Quart. J. Roy. Met. Soc. 80*, 131–164.

Betts, A. K. 1982. Saturation point analysis of moist convective overturning. *J. Atmos. Sci. 39*, 1484–1505.

Businger, S. 1985. The synoptic climatology of polar low outbreaks. *Tellus 37A*, 419–432.

Charney, J. G. and Eliassen, A. 1964. On the growth of the hurricane depression. *J. Atmos. Sci. 21*, 68–75.

Emanuel, K. A. 1986. An air–sea interaction theory for tropical cyclones. Part I: Steady-state maintenance. *J. Atmos. Sci. 43*, 585–604.

Emanuel, K. A. 1988. The maximum intensity of hurricanes. *J. Atmos. Sci. 45*, 1143–1155.

Grønås, S., Foss, A. and Lystad, M. 1987. Numerical simulations of polar lows in the Norwegian Sea. *Tellus 39A*, 334–353.

Harrold, J. W. and Browning, K. A. 1969. The polar low as a baroclinic disturbance. *Quart. J. Roy. Met. Soc. 95*, 710–723.

Large, W. G. and Pond, S. 1982. Sensible and latent heat flux measurements over the ocean. *J. Phys. Ocean. 12*, 464–482.

Louis, J.-F. 1979. A parametric model of vertical eddy fluxes in the atmosphere. *Boundary Layer Meteorol. 17*, 187–202.

Nordeng, T. E. 1987. The effect of vertical and slantwise convection on the simulation of polar lows. *Tellus 39A*, 354–375.

Ooyama, K. 1964. A dynamical model for the study of tropical cyclone development. *Geofis. Int. 4*, 187–198.

Rasmussen, E. 1979. The polar low as an extratropical CISK disturbance. *Quart. J. Roy. Met. Soc. 105*, 531–549.

Rasmussen, E. 1985. A case study of a polar low development over the Barents Sea. *Tellus 37A*, 407–418.

Reed, R. J. 1979. Cyclogenesis in polar airstreams. *Mon. Weather Rev. 107*, 38–52.

Rotunno, R. and Emanuel, K. A. 1987. An air–sea interaction theory for tropical cyclones. Part II: Evolutionary study using a nonhydrostatic axisymmetric numerical model. *J. Atmos. Sci. 44*, 542–561.

Sardie, J. M. and Warner, T. T. 1985. A numerical study of the development mechanism of polar lows. *Tellus 37A*, 460–477.

Shapiro, M. A., Fedor, L. S. and Hampel, T. 1987. Research aircraft measurements of a polar low over the Norwegian Sea. *Tellus 39A*, 272–306.

Staley, D. O. and Gall, R. L. 1977. On the wavelength of maximum baroclinic instability. *J. Atmos. Sci. 34*, 1679–1688.